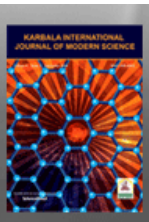

Karbala International Journal of Modern Science

Volume 11 | Issue 3 Article 6

Positive and negative parity states of 226-236Th isotopes

Ali A. Mezban
Department of Physics, College of Education for Pure Sciences, University of Basrah, Basrah, Iraq.

Falih H. Al-Khudair
Department of Physics, College of Education for Pure Sciences, University of Basrah, Basrah, Iraq., falih9@gmail.com

Recommended Citation

Mezban, Ali A. and Al-Khudair, Falih H. (2025) "Positive and negative parity states of 226-236Th isotopes," *Karbala International Journal of Modern Science*: Vol. 11 : Iss. 3 , Article 6.
Available at: https://doi.org/10.33640/2405-609X.3412

Positive and negative parity states of 226-236Th isotopes

Abstract

The level scheme of the $^{226-236}$Th nuclei is analyzed using the Interacting Boson Model (IBM-1). The ground state band (g. s.-band), beta band (β-band), gamma band (γ-band) have been described in the *sd* model space. To calculate the negative parity energy levels, the model space is extended to *sdf* by adding the *f*-boson (L=3). A sequence of states in energy bands up to 3.5 MeV has been obtained. The decay of negative states below 1 MeV built on an octupole vibration modes is investigated. The transition probabilities in-band and inter-band are calculated using the wave function of the levels. The potential energy surfaces (PES) values have been plotted to describe the nuclear shape. The model calculations are consistent with the available observed results

Keywords

Energy levels; Nuclear structure; Interacting boson model; Heavy nuclei; Thorium isotopes

Cover Page Footnote

Dear Editor I would like to inform you that the article proof is correct except for Q6 regarding Ref. 45. Please refer to paragraph 3.8, specifically to the sentence "For triaxial shapes, the value of γ provides insight into the rigidity or softness of the nuclear shape [45]." where the Ref 45 is placed instead of 44 With my best regards, Falih Al-Khuda

RESEARCH PAPER

Positive and Negative Parity States of $^{226\text{-}236}$Th Isotopes

Ali A. Mezban, Falih H. Al-Khudair*

Department of Physics, College of Education for Pure Sciences, University of Basrah, Basrah, Iraq

Abstract

The level scheme of the $^{226\text{-}236}$Th nuclei is analyzed using the Interacting Boson Model (IBM-1). The ground state band (g. s.-band), beta band (β-band), gamma band (γ-band) have been described in the *sd* model space. To calculate the negative parity energy levels, the model space is extended to *sdf* by adding the *f*-boson (L = 3). A sequence of states in energy bands up to 3.5 MeV has been obtained. The decay of negative states below 1 MeV built on an octupole vibration modes is investigated. The transition probabilities in-band and inter-band are calculated using the wave function of the levels. The potential energy surfaces (PES) values have been plotted to describe the nuclear shape. The model calculations are consistent with the available observed results.

Keywords: Energy levels, Nuclear structure, Interacting boson model, Heavy nuclei, Thorium isotopes

1. Introduction

The investigation of shape transitions of deformed heavy nuclei exhibits reflection-symmetric equilibrium shapes [1–4]. In these nuclei, the transition to low-lying octupole one-phonon states can also exhibit enhanced B(E1) rates. The appearance of the negative-parity bands contributed to the position of the shape transitions [5–7]. Experimentally, at low energy levels, the $J = 3^-$ state has been observed in both even–even spherical and weakly deformed nuclei, while $J = 1^-, 3^-, \ldots$ with $K = 0^-$ are found in strongly deformed nuclei [8]. For the nuclei around A = 230, the closely lying single particle $g_{9/2}$ and $j_{15/2}$ neutron orbitals, along with the $f_{7/2}$ and $i_{13/2}$ proton orbitals, in proximity to the Fermi level, form the basis for the existence of octupole deformation [9,10]. Using the inelastic scattering of charged particles, their collective octupole vibrational nature has been identified with B(E3) ↑ ≅ 10–30 W.u. It is found in some isotopes that the energy of the 3^- state lies higher than the 2_2^+ state, and B (E1; $3^- \rightarrow 2_2^+$) has been measured [11]. Nomura et al. studied the E1 transition by projecting the deformation axially symmetric onto the IBM Hamiltonian [12]. Experimental works in the rare-earth region suggest that stable octupole deformations exist at high angular momenta (J > 10) [13–18]. Several theoretical investigations of the nuclear structure of Th-isotopes have been carried out [19–27]. Recently, the stability and the hexadecapolar deformation effects as well as the dynamical deformation parameters (β2, β4)-coupling on the structure of the Th- isotopes have been investigated [28]. In the present study, special attention is paid to the position of negative parity states up to 3.5 MeV, some of which are generated by the *f*-boson, and to identifying their decay to low-lying positive parity states.

The aims of the present work are the following:

1. To calculate the energy spectrum of Thorium isotopes (A = 226–236) using IBM (*sdf*-boson space)
2. To study the transition probability between the energy levels, including the B(E1), B(E2), and B(E3) values.
3. To investigate the PES of the studied nuclei.

Received 17 March 2025; revised 8 June 2025; accepted 13 June 2025.
Available online 4 July 2025

* Corresponding author.
E-mail address: falih9@gmail.com (F.H. Al-Khudair).

https://doi.org/10.33640/2405-609X.3412

2. The model

In calculating the positive energy spectrum, the model Hamiltonian, which is written in the language of second quantization ($ss^\dagger$, $dd^\dagger$) where $ss^\dagger$ and $dd^\dagger$ are the annihilation and creation operators of s and d-bosons, respectively. The general form within one body and two body terms is written [29–32]:

$$V_{sdf}^{Mult} = A_1 L_d.L_f + A_2 Q_d \cdot Q_f - A_3 Q^3 \cdot Q^3. \tag{4}$$

$$L_d.L_f = -2\sqrt{210}\left[(d^\dagger \tilde{d})^{(1)} \times (f^\dagger \tilde{f})^{(1)}\right]_0^{(0)} \tag{5}$$

$$Q_d.Q_f = -2\sqrt{35}\left[\left\{(d^\dagger \tilde{s} + s^\dagger \tilde{d})^{(2)} - \chi (d^\dagger \tilde{d})^{(2)} \times (f^\dagger \tilde{f})^{(2)}\right]_0^{(0)} \tag{6}$$

$$\begin{aligned} H = {} & E_0 + \varepsilon_s (s^\dagger \cdot \tilde{s}) + \varepsilon_d \sum_\mu d_\mu^\dagger . \tilde{d}_\mu + \sum_{L=0.2.4} \frac{1}{2}\sqrt{2L+1}\, C_L \left[(d^\dagger \times d^\dagger)^{(L)} \times (\tilde{d} \times \tilde{d})^{(L)}\right]_0^{(0)} + \frac{1}{\sqrt{2}} \tilde{\nu}_2 \left[(d^\dagger \times d^\dagger)^{(2)} \times (\tilde{d} \times \tilde{s})^{(2)}\right. \\ & \left. + (d^\dagger \times s^\dagger)^{(2)} \times (\tilde{d} \times \tilde{d})^{(2)}\right]_0^{(0)} + \frac{1}{2} \tilde{\nu}_0 \left[(d^\dagger \times d^\dagger)^{(0)} \times (\tilde{d} \times \tilde{s})^{(0)} + (s^\dagger \times s^\dagger)^{(2)} \times (\tilde{d} \times \tilde{d})^{(0)}\right]_0^{(0)} \\ & + u_2 \left[(d^\dagger \times s^\dagger)^{(2)} \times (\tilde{d} \times \tilde{s})^{(2)}\right]_0^{(0)} + \frac{1}{2} u_0 \left[(s^\dagger \times s^\dagger)^{(0)} \times (\tilde{s} \times \tilde{s})^{(0)}\right]_0^{(0)} \end{aligned} \tag{1}$$

Another form often used can be written in the following multiple formal [33]:

$$\begin{aligned} \tilde{H} = {} & \varepsilon_d \tilde{n}_d + a_0 \tilde{P} \cdot \tilde{P} + a_1 \tilde{L} \cdot \tilde{L} + a_2 \tilde{Q} \cdot \tilde{Q} + a_3\, \tilde{T}_3 \cdot \tilde{T}_3 \\ & + a_4 \tilde{T}_4 \cdot \tilde{T}_4 \end{aligned} \tag{2}$$

where the coefficients $a_i (i = 0-4)$ are a linear component for the coefficients in Eq. (1), and;

$\tilde{n}_d = (\tilde{d}^\dagger \cdot \tilde{d})$: the number of d − boson operator.

$\tilde{P} = \frac{1}{2}[(\tilde{d} \cdot \tilde{d}) - (\tilde{s} \cdot \tilde{s})]$: the paring operator.

$\tilde{L} = \sqrt{10}[d^\dagger \times \tilde{d}]^{(1)}$: the angular momentum operator.

$\tilde{Q} = [d^\dagger \times \tilde{s} + s^\dagger \times \tilde{d}]^{(2)} + \chi[\tilde{d} \times \tilde{d}^\dagger]^{(2)}$ the quadrupole operator

$\tilde{T}_l = [\tilde{d}^\dagger \tilde{d}]^{(l)}$ $(l = 3.4)$: the octupole and hexadecapolar operators.

To calculate negative-parity energy levels, the space can be extended to include the f-boson $(l = 3)$, thus the Hamiltonian of the system becomes as follows [34–39]:

$$H = H_{sd} + H_f + V_{sdf}\ . \tag{3}$$

H_{sd} the Hamiltonian in *sd*-space interaction as in Eq. (2). $H_f = E_f n_f$, where n_f and E_f are the number operator and energy for f-boson. V_{sdf} describes boson's interaction in *sdf*-space. The multipole expansion has been used in the form

$$Q^3 = \left(s^\dagger \tilde{f} + f^\dagger \tilde{s}\right)^{(3)} - \chi_3 \left(d^\dagger \tilde{f} + f^\dagger \tilde{d}\right)^{(3)} \tag{7}$$

The electric transition operator $T^{(EL)}$ $(L = 1, 2, 3)$ in the IBM has the following form:

$$T^{E1} = e_{1Q}\left[T^{E2} \times \left(s^\dagger \tilde{f} + f^\dagger \tilde{s}\right)^{(3)}\right]^{(1)} + e_{1df}\left(d^\dagger \tilde{f} + f^\dagger \tilde{d}\right)^{(1)} \tag{8}$$

$$T^{E2} = e_{2sd}\,(d^\dagger \tilde{s} + s^\dagger \tilde{d})^{(2)} + e_{2dd}(d^\dagger \tilde{d})^{(2)} \tag{9}$$

$$\begin{aligned} T^{E3} = {} & e_{3Q}\left[T^{E2} \times \left(s^\dagger \tilde{f} + f^\dagger \tilde{s}\right)^{(3)}\right]^{(3)} \\ & + e_{3sf}\left(s^\dagger \tilde{f} + f^\dagger \tilde{s}\right)^{(3)} + e_{3df}\left(d^\dagger \tilde{f} + f^\dagger \tilde{d}\right)^{(3)} \end{aligned} \tag{10}$$

The basic concepts of nuclear structure can be clarified by carefully describing the PES. Using deformation parameters β and γ, the PES formal as follows [40,41]:

$$\begin{aligned} V(\beta.\gamma) = {} & \frac{N_B}{1+\beta^2}\left(R_1 + R_2\beta^2\right) \\ & + \frac{N_B(N_B-1)}{\left(1+\beta^2\right)^2}\left(R_3\beta^4 + R_4\beta^3\, cos\, 3\,\gamma + R_5\beta^2 + R_6\right) \end{aligned} \tag{11}$$

where R_i is related to the model Hamiltonian in *sd*-space parameters [33]. N_B is boson number.

3. Results and discussion

The energy levels were investigated by determining the model Hamiltonian parameters defined in Eq. (3). The value of the ratio $R_{4/2} = E(4_1^+)/E(2_1^+)$ shows that the $^{226\text{-}236}$Th isotopes belong to the SU(3) limit as shown in Table 1. Therefore, the energy spectrum depends on the $L.L$ and $Q.Q$ terms in the Hamiltonian, and the boson energy vanishes,

Table 1. The value of the energy ratio $R_{4/2} = E(4_1^+)/E(2_1^+)$ of $^{226\text{-}236}Th$ isotopes.

A	EXP	IBM
226	3.13	3.33
228	3.26	3.31
230	3.28	3.33
232	3.34	3.37
234	3.32	3.37
236	3.33	3.37

meaning that $V_{ij} >> \varepsilon_d$ [33]. As pointed out in model theory, one can calculate the value of the parameters using the energy value of the 2_1^+ state. After examining the effect of each parameter value on the energy spectrum, the used values are tabulated in Table 2. The energy states are plotted up to the energy range of 3.5 MeV in Figs. 1–6.

3.1. Energy spectrum of the ^{226}Th isotope

This isotope has 136 neutrons, which means there are 4 proton bosons and 5 neutron bosons based on the closed shells of Z = 82 and N = 126, giving a total boson number of 9. Fig. 1 shows a comparison between the available experimental and theoretical results for the energy levels with three positive-parity bands, which are the ground band (g-band),

Table 2. The parameter values of the Hamiltonian used in Eq. (3). $\chi = -1.322$ for all isotopes.

A	N_B	a_1	a_2	A_1	A_2	A_3
226	9	0.005	−0.017	0.030	−0.010	−0.010
228	10	0.005	−0.012	0.010	−0.010	−0.012
230	11	0.004	−0.013	0.018	−0.010	−0.020
232	12	0.004	−0.011	0.010	−0.010	−0.029
234	13	0.004	−0.011	0.010	−0.010	−0.024
236	14	0.004	−0.010	0.010	−0.010	−0.020

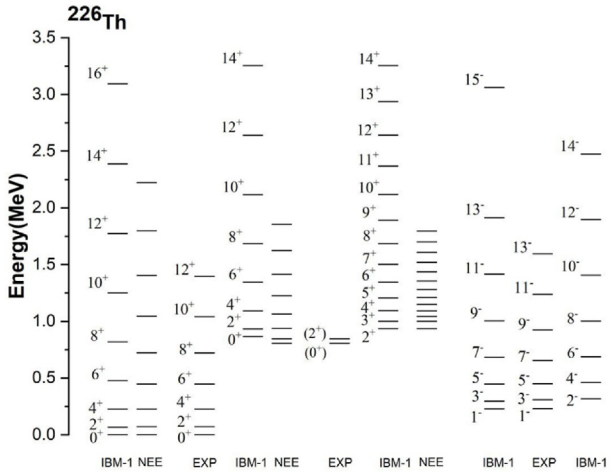

Fig. 1. Theoretical and available experimental energy levels for the ^{226}Th isotope.

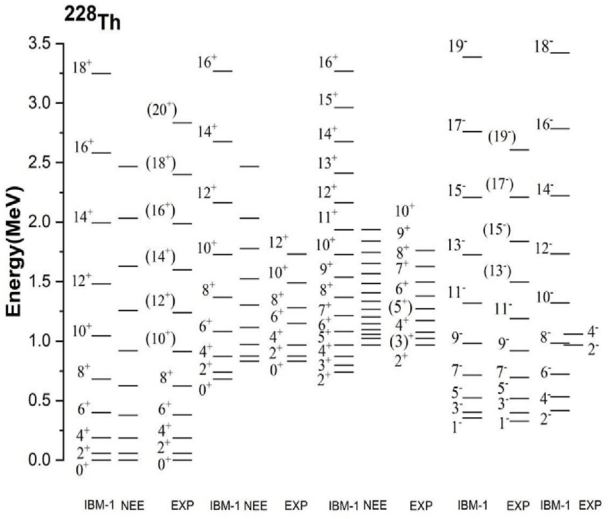

Fig. 2. Theoretical and available experimental energy levels for the ^{228}Th isotope.

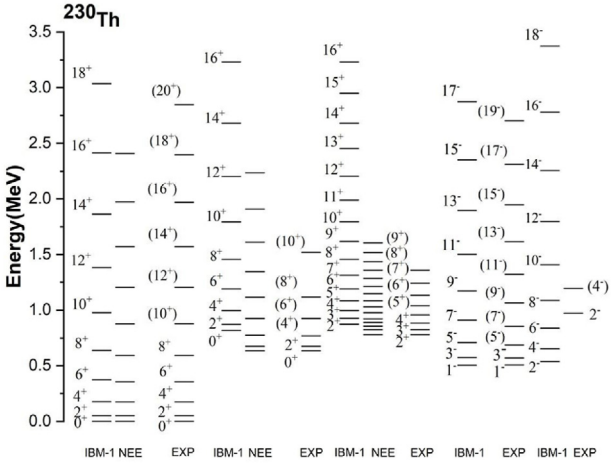

Fig. 3. Theoretical and available experimental energy levels for the ^{230}Th isotope.

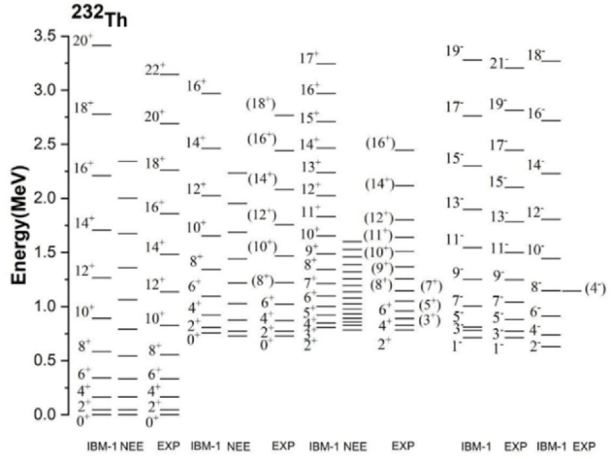

Fig. 4. Theoretical and available experimental energy levels for the ^{232}Th isotope.

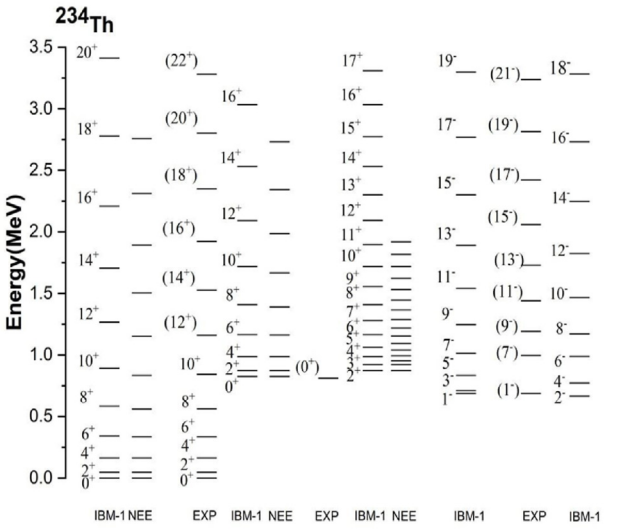

Fig. 5. Theoretical and available experimental energy levels for the ^{234}Th isotope.

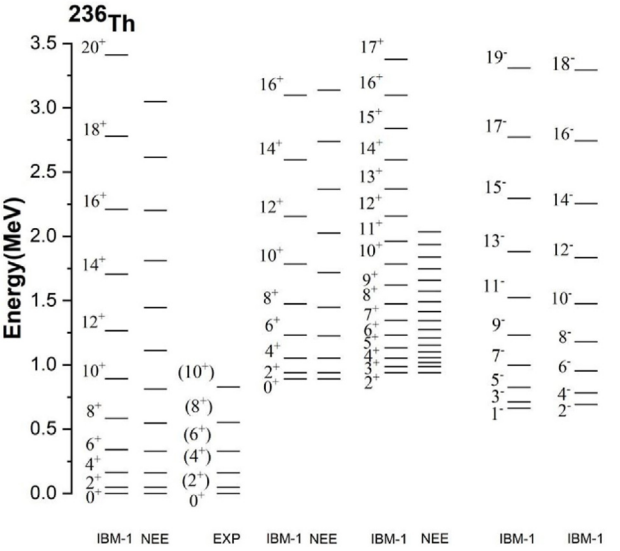

Fig. 6. Theoretical and available experimental energy levels for the ^{236}Th isotope.

the gamma band (γ-band), the beta band (β-band), and two negative-parity bands. Experimental data were obtained from Ref. [42]. From the comparison between the calculated values and the experimental results of the ground state band levels ($J = 2^+$- 8^+), it was found that the difference in energy is equal to (0.004–0.097 MeV). For example, for the 8^+ state, the theoretical energy value is 0.818 MeV, while the experimental value is 0.721 MeV. The energy difference of the ground band levels increases with increasing value of angular momentum. As for the β-band levels, the energy of its head 0_2^+ state is equal to 0.805 MeV and 0.866 MeV in the experimental and model results. According to model results, the γ-band head of the 2_3^+ state appears at 0.935 MeV, followed by the 3_1^+ state with an energy of 1.003 MeV. The figure includes negative-parity bands, including the first band ($J = 1^-, 3^-,\ldots\ \ldots, 15^-$). The experimental and theoretical values agree well up to the 9^- state. For example, the 5^- state has an experimental energy of 0.450 MeV, while its theoretical energy is 0.446 MeV. The levels of the second band, whose head shows a 2^- state with an energy level of 0.318 MeV in IBM results, are not observed.

3.2. Energy spectrum of the ^{228}Th isotope

As the number of neutrons increases, the total number of bosons becomes 10. This number gives a wide range, calculating a large number of excited levels, reaching $J = 20^+$. Fig. 2 shows a comparison between the available experimental [41] and the model results. A slight difference was found between the predicted and observed energy values for the ground band levels ($J = 2^+$-10^+). For example, the observed energy for the 6^+ level is 0.378 MeV, and theoretical energy is 0.398 MeV, i.e., a difference of 0.02 MeV.

The energy of the 10^+ level is equal to 0.911 MeV and 1.044 MeV in the experimental and model results, respectively. For the β-band, its head, the 0^+ state, is located significantly above the first excited state with an energy of 0.831 MeV and 0.684 MeV experimental and model results. The difference in energy of the other levels increases, as shown in the figure. Likewise, in the γ-band, the energy values of the theoretical levels are higher than the experimental ones. A good agreement in the energy of the 10_1^+ level has been found where its energy is equal to 1.729 MeV and 1.761 MeV in IBM and observed data, respectively. The energy values of negative-parity states ($J = 1^-, 3^-,\ldots\ \ldots 19^-$) are shown in the figure. Experimentally, the energy values of the levels $J = 1^-, 3^-$, $5^-, 7^-$ 9^- are 0.328, 0.396, 0.519, 0.695, and 0.920 MeV, while the predicted one is equal to 0.355, 0.403, 0.523, 0.716, and 0.981 MeV. The first two levels, $J = 2^-$ and 4^-, in the second band, are measured with energies of 0.968 MeV and 1.059 MeV, far from their theoretical appearance with energies of 0.417 MeV and 0.533 MeV. Therefore, they can be considered outside the used *sdf* space and may be generated from the *p*-boson ($L = 1$) in coupling with *sd*-space excitations.

3.3. Energy spectrum of the ^{230}Th isotope

The model results and the observed data for the five bands are compared in Fig. 3. For the β-band,

we find that the energy values for the J = 0_2^+ level are equal to 0.819 MeV and 0.634 MeV, and for the 2_2^+ level they are equal to 0.872 MeV and 0.677 MeV, theoretically and experimentally, respectively. The energy difference between the two levels is close, as is the case for the other levels. For the γ-band, we find that the theoretical energy value of its levels is less than the experimental ones [39]. Negative parity states were calculated for two bands within the energy range. A great convergence in the values of the first band, where the energy of the J = 1^-, 3^-, 5^-, 7^-, 9^-, 11^- levels was practically equal to 0.508, 0.571, 0.686, 0.852, 1.065, 1.322 MeV, and theoretically equal to 0.506, 0.575, 0.709, 0.909, 1.173, 1.502 MeV.

The energy deviation increases with spin (J) increases. As for the second band, it is characterized by the same behavior as in the previous isotope, where the energy values of the 2^- and 4^- levels are equal to 0.971, 1.196 MeV, and 0.540, 0.653 MeV experimentally and theoretically, respectively.

3.4. Energy spectrum of the ^{232}Th isotope

This isotope has 142 neutrons, so the number of neutron bosons is 8, and N_B = 12. The energy spectrum is plotted in Fig. 4. The levels of the ground band were drawn up to the J = 20^+ level. The energy of the 6^+ state is equal to 0.333 MeV and 0.341 MeV in the experimental and model results, respectively. From the figure, it can be seen that for the 8^+ state, the difference in energy is equal to 0.028 MeV. While the energy of 12^+ states is equal to 1.267 MeV and 1.137 MeV theoretically and experimentally, respectively. The negative parity energy levels were calculated up to the J = 19^- level, and a great convergence appeared in the energy values of the first band up to the J = 11^- level. The energy values of the J = 1^-, 3^-, 5^-, 7^-, 9^-, 11^- levels were equal to 0.714, 0.774, 0.883, 1.042, 1.249, 1.498 MeV in practice and equal to 0.713, 0.783, 0.813, 1.006, 1.250, 1.546 MeV. The energy of the levels of theory begins to move away from the experimental values. Experimentally, there is a level at 1.143 MeV. In the model calculation, it was found that the energy of the first appearance of the level is 0.739 MeV. Therefore, this level is not among the members of the calculated band.

3.5. Energy spectrum of the ^{234}Th isotope

The comparison between theoretical and available experimental results has been shown in Fig. 5. The $E(6_1^+)$ level equals 0.336 and 0.341 MeV for the model and experimental results, respectively. There is a difference in the energy levels with high angular momentum J > 12^+. Theoretically, the head of the β-band (0_2^+) level appears at 0.825 MeV is close to observed one at 0.810 MeV. Regarding the γ-band, it was found that the $E(2_3^+)$ level is close to the energy value of the 3_1^+ level, with calculated energies of 0.874 MeV and 0.922 MeV, respectively. The remaining levels appear in sequence extending up to the J= 17^+ level with an energy equal to 3.311 MeV. For the first negative parity band, the energy of the J = 1^- state is equal to 0.727 MeV and 0.688 MeV, theoretically and practically, respectively. While the 7^- state appeared with a theoretical energy of 1.033 MeV compared to experimental value of 0.995 MeV.

3.6. Energy spectrum of the ^{236}Th isotope

Fig. 6 shows a comparison between theoretical and available experimental energy levels. Experimentally, only J ≤ 10_1^+ levels of the ground state band have been measured. Good agreement is observed between theoretical and experimental values for these levels, as their energy values were 0.049, 0.162, 0.341, 0.585, 0.894 MeV according to theoretical results and 0.048, 0.160, 0.329, 0.553, 0.826 MeV according to experimental results. The energy difference equals 0.002 MeV for the 4_1^+ level and 0.012 MeV for the 6_1^+ level. Theoretically, the β- and γ-band head show 0_2^+ and 2_3^+ levels with energies equal to 0.891 MeV and 0.941 MeV, respectively. Moreover, the head of the two negative parity bands 1^- and 2^- levels, appeared with energies equal to 0.661 MeV and 0.691 MeV, respectively.

In addition, a simplified calculation approach has been attempted using a new empirical equation (NEE) as introduced in Ref. [43] for g. s. band defend as:

$$E(J) = \frac{C_1 J(J+1)}{C_2(J+1) + J^{C_3}}$$

and

$$E(J) = E_0 + \frac{(C_1 + B)J(J+1)}{C_2(J+1) + J^{C_3}}$$

for β and γ bands. The C_1, C_2, C_3 and B parameters are calculated by analyzing the low-lying experimental levels for each band as listed in Table 3. For $^{234,\ 236}$ Th isotopes, the value of the B parameter values have been calculated by fitting the IBM calculation of the first two members of the β and γ bands. The NEE results are plotted in Figs. 1–6. It is found that all energies are close to experimental ones in g. s. and β bands. On the other hand, there is a disagreement in energies of γ-band members. The

Table 3. The values of the NEE parameters of the g. s., β and γ bands in MeV unit for the $^{226,\ 236}$ Th isotopes.

	C_1	C_2	C_3	B_β	B_γ
226	0.0133	0.0391	−0.0140	−0.0055	−0.0069
228	0.0099	0.0265	−0.0463	−0.0024	−0.0052
230	0.0091	0.0218	−0.0418	−0.0017	−0.0053
232	0.0084	0.0406	−0.1428	−0.0008	−0.0046
234	0.0083	0.0273	−0.0604	0.0007	−0.0042
236	0.0082	0.0247	−0.0773	0.0002	−0.0041

value of the *B* parameter values have been calculated by fitting the IBM calculation of the first two members β and γ bands.

3.7. Electric transition probabilities

The B(E2) transition probabilities have been calculated using Eq. (9). The parameter values were determined by fitting the experimental data [42] of the B(E2; $2_1^+ \rightarrow 0_1^+$), where $e_{2sd} = 0.183$, 0.186, 0.202, 0.210, 0.198, and 0.200 *e b* for $^{226\text{-}236}$Th nuclei, respectively. The values have been listed in Tables 4 and 5. Regarding the transitions $J^+ \rightarrow J^+ - 2$ in the ground state band, The B(E2) values increase with increasing angular momentum up to $J = 8^+$. The calculated B(E2) values for the ground state band show reasonable agreement with experimental data. We note that the weakest transitions occur from γ-band members to the ground-state band. This feature is well described by the IBM theory [33]. For the ^{230}Th isotope, the calculated B(E2; $2_\gamma^+ \rightarrow 2_1^+$) is equal to 0.0197 $e^2\ b^2$ compared to the experimental data $0{\cdot}047^{+84}_{-61}$ $e^2\ b^2$. The B(E2; $4_2^+ \rightarrow 2_2^+$) is greater than the B(E2; $3_1^+ \rightarrow 2_2^+$). This is because the two states are members of the β-band, i.e., the first transition is in-band.

Table 4. Theoretical B(E2) values for $^{226\text{-}230}$Th isotopes in (e^2b^2) unit. Available observed data [42] is provided in the second row.

$J_i^+ \rightarrow J_f^+$	^{226}Th	^{228}Th	^{230}Th
$2_1 \rightarrow 0_1$	1.3404	1.4450	1.6332
	1.3438(819)		1.6441(503)
$4_1 \rightarrow 2_1$	1.8929	2.0404	2.3063
			2.2228(755)
$6_1 \rightarrow 4_1$	2.0411	2.2002	2.4869
$8_1 \rightarrow 6_1$	2.0704	2.2319	2.5227
$10_1 \rightarrow 8_1$	2.0378	2.1967	2.4829
$2_2 \rightarrow 0_2$	0.0098	0.0106	0.0120
$2_2 \rightarrow 2_1$	0.1018	0.1097	0.1240
$2_3 \rightarrow 2_1$	0.0162	0.0174	0.0197
			$0{\cdot}0461^{+84}_{-67}$
$2_3 \rightarrow 2_2$	0.0104	0.0112	0.0127
$4_2 \rightarrow 2_2$	0.6954	0.7499	0.8476
$3_1 \rightarrow 2_1$	0.1143	0.1232	0.1393
$3_1 \rightarrow 2_2$	0.0160	0.0172	0.0194
$3_1 \rightarrow 4_1$	0.0580	0.0626	0.0707
$5_1 \rightarrow 3_1$	1.0997	1.1854	1.3399
$5_1 \rightarrow 4_1$	0.0917	0.0989	0.1117

Table 5. Theoretical B(E2) values for $^{232\text{-}236}$Th isotopes unit. Available observed data [42] is provided in the second row.

$J_i^+ \rightarrow J_f^+$	^{232}Th	^{234}Th	^{236}Th
$2_1 \rightarrow 0_1$	1.7652	1.5692	1.6011
	1.6801(933)	1.5707(1373)	
$4_1 \rightarrow 2_1$	2.4926	2.2159	2.2609
	2.4268(2037)		
$6_1 \rightarrow 4_1$	2.6878	2.3894	2.4379
	2.7663(1867)		
$8_1 \rightarrow 6_1$	2.7265	2.4238	2.4730
	2.9190(1273)		
$10_1 \rightarrow 8_1$	2.6834	2.3855	2.4340
	3.0002(1782)		
$2_2 \rightarrow 0_2$	0.0129	0.0116	0.0118
$2_2 \rightarrow 2_1$	0.1341	0.1192	0.1216
	0.0042(14)		
$2_3 \rightarrow 2_1$	0.0213	0.0189	0.0193
	0.0611(59)		
$2_3 \rightarrow 2_2$	0.0130	0.0120	0.0123
$4_2 \rightarrow 2_2$	0.9161	0.8144	0.8310
$3_1 \rightarrow 2_1$	0.1505	0.1338	0.1365
$3_1 \rightarrow 2_2$	0.0210	0.0187	0.0190
$3_1 \rightarrow 4_1$	0.0764	0.0679	0.0693
$5_1 \rightarrow 3_1$	1.4481	1.2873	1.3135
$5_1 \rightarrow 4_1$	1.1208	1.1074	1.1095

The values of the E1 operator parameters were adjusted to reproduce the B(E1; $3_1^- \rightarrow 2_1^+$) value observed in the ^{232}Th, where $e_{1Q} = 0.0005\ e\ b^{1/2}$ and $e_{1df} = 0.0007\ e\ b^{1/2}$ for all isotopes. The calculated values indicated a variation in the mass number, suggesting a change in the n_d value of the 3_1^- state structure, where the 2_1^+ state corresponds to $s^N\ d^1$ bosons. In Tables 6 and 7, we listed IBM B(E1) values. Regarding the electric properties, B(E3) has been calculated. Tables 6 and 7 have shown IBM B(E3) values for $^{226\text{-}236}$Th isotopes. The values of the e_{3Q} and e_{3sf} in the E3 operator are estimated by fitting the observed B(E3; $3_1^- \rightarrow 0_1^+$) in the ^{230,232}Th isotopes.

The $e_{3Q} = 0.5$, 0.43, 0.55, 0.55, 0.32, and 0.3 $e\ b^{3/2}$, while $e_{3sf} = 0.3\ e\ b^{3/2}$ is taken for all isotopes. From these tables, it can be seen that the 1_1^- and 2_1^+ states are connected by a very strong E3 transition in the ^{228,232}Th nuclei, showing that the initial state is a full *1f*-boson component. The B(E2) ratios can be used to distinguish between the nuclear shapes by their value of model limit. One can apply the following B(E2) ratios [44].

$$R_1 = \frac{2_2^+ \rightarrow 0_1^+}{2_2^+ \rightarrow 2_1^+}, R_2 = \frac{2_2^+ \rightarrow 2_1^+}{2_1^+ \rightarrow 0_1^+},$$

$$R_3 = \frac{4_1^+ \rightarrow 2_1^+}{2_2^+ \rightarrow 2_1^+}, R_4 = \frac{3_1^+ \rightarrow 2_1^+}{3_1^+ \rightarrow 4_1^+}$$

Table 6. IBM B(E1) and B(E3) in e^2b and $e^2\ b^3$ unit, respectively, for $^{226\text{-}230}$Th. Available observed data [42] is provided in the second row.

Transition	^{226}Th		^{228}Th		^{230}Th	
$J_i^- \rightarrow J_f^+$	B(E1)	B(E3)	B(E1)	B(E3)	B(E1)	B(E3)
$1_1 \rightarrow 0_1$	3.6×10^{-7}		1.7×10^{-5}		7.1×10^{-6}	
$1_1 \rightarrow 2_1$	1.3×10^{-5}	0.0852	1.9×10^{-6}	0.4351	1.1×10^{-5}	0.1901
$1_1 \rightarrow 4_1$		0.4478		0.0680		0.5640
$3_1 \rightarrow 0_1$		0.0014		0.1138		0.0929
						0.0914(85)
$3_1 \rightarrow 2_1$	1.1×10^{-7}	0.0125	1.7×10^{-5}	0.2085	1.9×10^{-6}	0.0270
$3_1 \rightarrow 4_1$	1.1×10^{-5}	0.1066	4.0×10^{-6}	0.1702	1.3×10^{-5}	0.1382
$2_1 \rightarrow 2_1$	1.0×10^{-5}	0.1372	1.3×10^{-5}	0.0098	1.4×10^{-5}	0.4493
$2_1 \rightarrow 4_1$		0.1129		0.2120		0.2195
$5_1 \rightarrow 4_1$	4.0×10^{-8}	0.0119	1.7×10^{-5}	0.2374	7.0×10^{-7}	0.0007
$5_1 \rightarrow 2_1$		0.0005		0.1348		0.0554
$4_1 \rightarrow 2_1$		0.0507		0.0121		0.1420
$4_1 \rightarrow 4_1$	8.2×10^{-7}	0.1802	1.1×10^{-5}	0.0479	1.0×10^{-5}	0.4315
$7_1 \rightarrow 4_1$		0.0429		0.1035		0.0279
$7_1 \rightarrow 6_1$	2.0×10^{-7}	0.0084	1.6×10^{-5}	0.2696	3.6×10^{-7}	0.0001

The calculated B(E2) ratios and IBM limits are listed in Table 8. From the table, one can see that the model value close to the SU(3) limit exhibits strong collective behavior and deformed shapes.

3.8. Potential energy surface

The potential energy surface (PES) was calculated using Eq. (11). The coefficients of this equation were calculated based on the Hamiltonian parameters shown in Table 2. In Fig. 7, the PES values are plotted as a function of β and γ deformation parameters. The γ deformation parameter determines the nature of the nuclear shape orientation, where $\gamma = 0^\circ$ (prolate shape), $\gamma = 60^\circ$ (oblate shape) and $0^\circ < \gamma < 60^\circ$ (triaxial shapes). For triaxial shapes, the value of γ provides insight into the rigidity or softness of the nuclear shape [45]. While the β deformation parameter in this equation is related to the Bohr Collective Model (BCM) through a distortion factor as $\beta_{IBM} \cong \frac{A}{2 \cdot 36 N_B} \beta_{BCM}$, where A is the mass number [46]. To investigate the nuclear shape, PES was calculated for β ranging from 0 to 3, at fixed γ values of for $\gamma = 0^\circ$, 30° and 60° as shown in Fig. 8. Clearly, the V_{min} (β,γ) value is on the curve of $\gamma = 0^\circ$

Table 8. Calculated and IBM limit [44] values of the B(E2) ratio in Th isotopes.

R_i	^{226}Th	^{228}Th	^{230}Th	^{232}Th	^{234}Th	^{236}Th	U(5)	SU(3)	O(6)
R_1	0.64	0.61	0.64	0.64	0.64	0.64	0.01	0.70	0.07
R_2	0.07	0.07	0.07	0.07	0.07	0.07	1.40	0.02	0.79
R_3	18.59	18.59	18.59	18.58	18.58	18.59	1.0	6.93	1.84
R_4	1.97	1.97	1.97	1.97	1.97	1.97	0.06	2.5	0.12

Table 7. IBM B(E1) and B(E3) in e^2b and $e^2\ b^3$ unit, respectively for $^{232\text{-}236}$Th. Available observed data [42] is provided in the second row.

Transition	^{232}Th		^{234}Th		^{236}Th	
$J_i^- \rightarrow J_f^+$	B(E1)	B(E3)	B(E1)	B(E3)	B(E1)	B(E3)
$1_1 \rightarrow 0_1$	1.8×10^{-5}		2.6×10^{-5}		3.6×10^{-5}	
$1_1 \rightarrow 2_1$	4.0×10^{-6}	0.7634	3.3×10^{-6}	0.1864	1.3×10^{-6}	0.2792
$1_1 \rightarrow 4_1$		0.1908		0.0156		0.0027
$3_1 \rightarrow 0_1$		0.0758		0.0528		0.0308
		0.0771(85)				
$3_1 \rightarrow 2_1$	5.6×10^{-8}	0.0160	4.5×10^{-6}	0.0265	3.3×10^{-5}	0.1417
	$7.5\ (2.2) \times 10^{-8}$					
$3_1 \rightarrow 4_1$	9.0×10^{-8}	0.3537	4.0×10^{-7}	0.3196	3×10^{-5}	0.2184
	$8.0\ (10) \times 10^{-7}$					
$2_1 \rightarrow 2_1$	2.0×10^{-7}	0.2978	1.1×10^{-6}	0.2768	1.9×10^{-5}	0.0446
$2_1 \rightarrow 4_1$		0.2157		0.1952		0.2982
$5_1 \rightarrow 4_1$	2.4×10^{-7}	0.1738	1.4×10^{-5}	0.1653	3.4×10^{-5}	0.2054
$5_1 \rightarrow 2_1$		0.0109		0.0010		0.0657
$4_1 \rightarrow 2_1$		0.1517		0.1512		0.0550
$4_1 \rightarrow 4_1$	7.8×10^{-7}	0.0225	3.6×10^{-6}	0.0182	1.8×10^{-5}	0.0018
$7_1 \rightarrow 4_1$		0.0088		0.0063		0.0710
$7_1 \rightarrow 6_1$	6.4×10^{-6}	0.3728	1.9×10^{-5}	0.2347	3.5×10^{-5}	0.2424

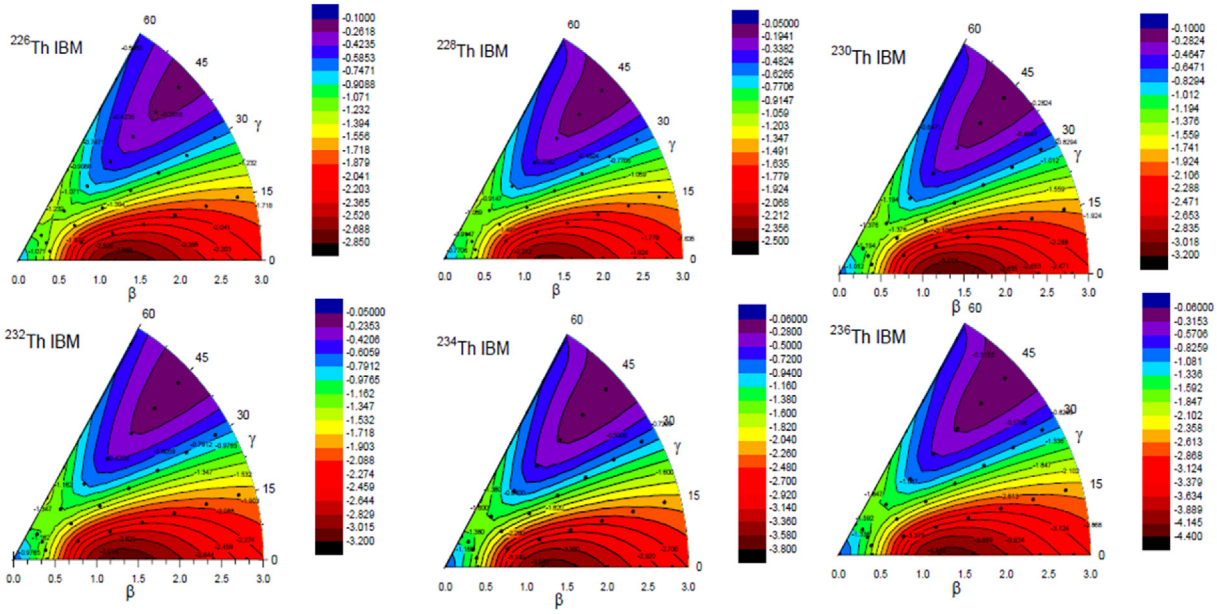

Fig. 7. The IBM PES for the $^{226\text{-}236}$Th isotopes, within deformation parameters: $0^\circ \leq \gamma \leq 60^\circ$ and $0 \leq \beta_2 \leq 3$.

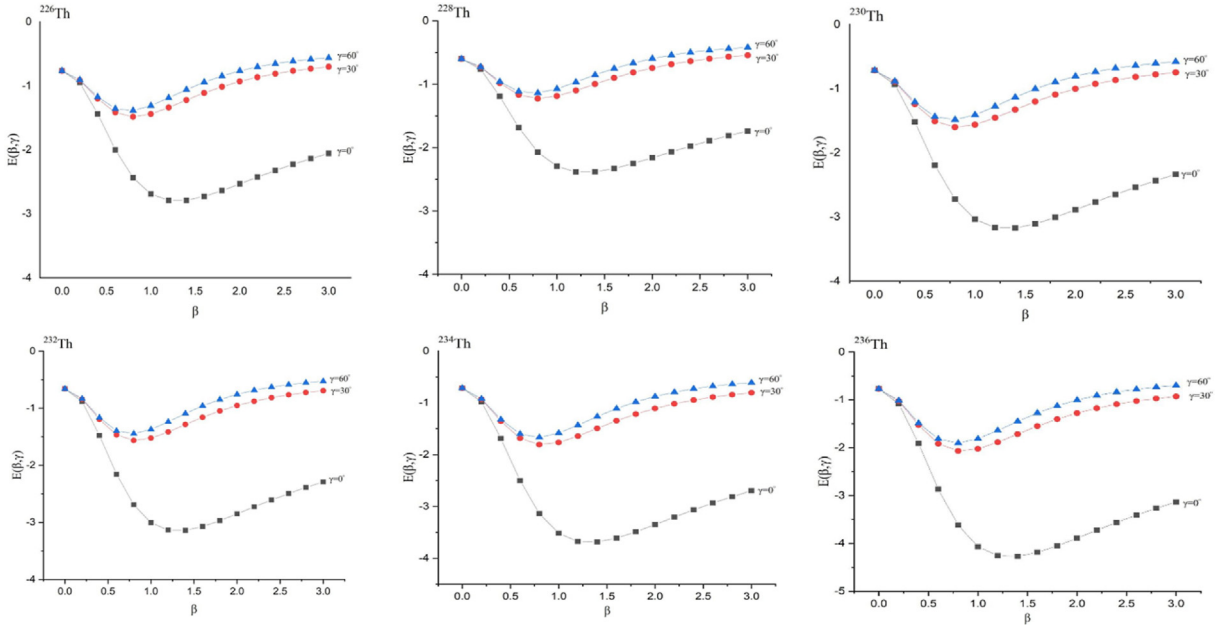

Fig. 8. The PES values as a function of $0 \leq \beta_2 \leq 3$ and $\gamma = 0^\circ$, 30°, and 60° for $^{226\text{-}236}$Th isotopes.

and it was as follows: V_{min} $(\beta,\gamma) = V_{min}$ $(1.2,0^\circ) = -2.7917$, $V_{min}(1.2,0^\circ) = -2.3847$, $V_{min} = (1.4,0^\circ) = -3.1726$, $V_{min}(1.4,0^\circ) = -3.1409$, $V_{min}(1.4,0^\circ) = -3.6853$ and $V_{min}(1.4,0^\circ) = -4.2732$ MeV for $^{226-236}$Th isotopes, respectively. These results indicate that the nuclei exhibit significant deformation and therefore fall within IBM's SU (3) limit mainly in a prolate shape.

4. Conclusion

The present investigation focuses on extending the model space to include the f-boson (L = 3). Two negative parity bands have been identified. The first band, built on the 1^- state, is interpreted as a *1f*-boson excitation. After the studying the energy spectrum, the PES shape agrees with the SU (3)

limit. The IBM describes the properties of the low-lying positive states without any additional parameters. For the negative parity states, this is not applicable to negative-parity states, which require additional degrees of freedom. As more negative-parity states are identified, including *p*-bosons (L = 1), they must be added to the model space. The root-mean-square deviations are very small with $\sigma = \left[\frac{1}{N}\sum (E_{Cal} - E_{Exp})^2\right]^{1/2}$, for example it is σ (g. s. band up $J = 12^+$) = 0.034, 0.017, 0.061, 0.085, 0. 115, and 0.181 for $^{226\text{-}236}$Th isotopes, respectively. Further refinement of the model may be achieved by incorporating triaxiality and cubic interaction and by adding the $Q \times Q \times Q$ term to the Hamiltonian will improve the model results for β **and** γ **bands.** The present study of the nuclear structure shows some interesting properties that need to be investigated, such as the abnormal behavior of the negative parity states. Further investigations of shape coexistence and octupole vibration would be more beneficial of helpful to complete the results of this work, especially in models based on dynamical deformation parameters (β2, β4)-coupling. The calculated results can serve as a valuable reference for experimentalists. Additional experimental studies will be necessary to further validate the current model calculations. In particular, more measurements of E1 transitions are needed to guide theoretical interpretations identify the structure of levels.

Ethics information

We certify that we have read the Journal's "Publication Ethics." We understand that the corresponding author is the sole contact for the editorial process.

Funding

This work did not receive any external funding.

Conflicts of interest

The authors declare that they have no competing interests.

Acknowledgment

The authors would like to thank the University of Basrah for their cooperation in realizing the present work.

References

[1] W. Nazarewicz, P. Olanders, I. Ragnarsson, J. Dudek, G.A. Leander P. Möller, E. Ruchowsa, Analysis of octupole instability in medium-mass and heavy nuclei, Nucl. Phys. A 429 (1984) 269–295, https://doi.org/10.1016/0375-9474(84)90208-2.

[2] S. Ćwiok, W. Nazarewicz, Reflection-asymmetric shapes in transitional odd- A Th isotopes, Phys. Lett. B 224 (1989) 5–10, https://doi.org/10.1016/0370-2693(89)91039-3.

[3] M. Chen, T. Li, J. Dobaczewski, W. Nazarewicz, Microscopic origin of reflection-asymmetric nuclear shapes, Phys. Rev. C 103 (2021) 034303-10, https://doi.org/10.1103/PhysRevC.103.034303.

[4] P.A. Butler, Studies of reflection asymmetry in heavy nuclei, Phys. Scr. 99 (2024) 035302-10, https://doi.org/10.1088/1402-4896/ad22c9.

[5] K. Nomura, T. Otsuka, N. Shimizu, L. Guo, Microscopic formulation of the interacting boson model for rotational nuclei, Phys. Rev. C 83 (2011), https://doi.org/10.1103/PhysRevC.83.041302, 041302(R)-5.

[6] A. Couture, R.F. Casten, R.B. Cakirli, Extended tests of an SU(3) partial dynamical symmetry, Phys. Rev. C 91 (2015) 014312-5, https://doi.org/10.1103/PhysRevC.91.014312.

[7] J.W. Cui, X.R. Zhou, F.Q. Chen, Y. Sun, C.L. Wu, Z.C. Gao, Description of collective and quasiparticle excitations in deformed actinide nuclei: the first application of the multi-shell shell model for heavy nuclei, Phys. Rev. C 90 (2014) 014321-8, https://doi.org/10.1103/PhysRevC.90.014321.

[8] P.A. Butler, W. Nazarewicz, Intrinsic reflection asymmetry in atomic nuclei, Rev. Mod. Phys. 68 (1996) 349–421, https://doi.org/10.1103/RevModPhys.68.349.

[9] S. Cwiok, W. Nazarewicz, Reflection-asymmetric shapes in odd-A actinide nuclei, Nuc1.Phys. A 529 (1991) 95–114, https://doi.org/10.1016/0375-9474(91)90787-7. https://www.sciencedirect.com/science/article/pii/0375947491907877.

[10] P. A. Buter, W. Nazarewicz, Intrinsic dipole moments in reflection-asymmetric nuclei, Nucl. Phys. A 533 (1991) 249–268, https://doi.org/10.1016/0375-9474(91)90489-S. https://www.sciencedirect.com/science/article/pii/037594749190489S.

[11] B. Buck, A.C. Merchant, S.M. Perez, Exotic clustering in ^{222,224,226}Ra, Nucl, Phys. A 617 (1997) 195–210, https://doi.org/10.1016/S0375-9474(97)00043-2.

[12] K. Nomura, D. Vretenar, T. Niksic, B.N. Lu, Microscopic description of octupole shape-phase transitions in light actinide and rare-earth nuclei, Phys. Rev. C 89 (2014) 24312–24316, https://doi.org/10.1103/PhysRevC.89.024312.

[13] G.A. Leander, W. Nazarewicz, G.F. Bertsch, J. Dudek, Low-energy collective E1 mode in nuclei, Nucl. Phys. A 453 (1986) 58–76, https://doi.org/10.1016/0375-9474(86)90029-1.

[14] W. Nazarewicz, P. Olanders, I. Ragnarsson, J. Dudek, G.A. Leander, P. Moller, E. Ruchowsa, Analysis of octupole instability in medium-mass and heavy nuclei, Nucl. Phys. A 429 (1984) 269–295, https://doi.org/10.1016/0375-9474(84)90208-2.

[15] W. Nazarewicz, Low energy octupole and dipole modes in nuclei, Nucl. Phys. A 520 (1990) c333–c351, https://doi.org/10.1016/0375-9474(90)91158-N.

[16] J.F.C. Cocks, D. Hawcroft, N. Amzal, P.A. Butler, K.J. Cann, P. T. Greenlees, G.D. Jones, S. Asztalos, R.M. Clark, M.A. Deleplanque, R.M. Diamond, P. Fallon, I.Y. Lee, A.O. Macchiavelli, R.W. Macleod, F.S. Stephens, P. Jones, R. Julin, R. Broda, B. Fornal, C.T. Zhang, Spectroscopy of Rn, Ra and Th isotopes using multi-nucleon transfer reactions, Nucl. Phys. A 645 (1999) 61–91, https://doi.org/10.1016/S0375-9474(98)00586-7.

[17] B.M. Loc, N. Le Anh, P. Papakonstantinou, N. Auerbach, Origin of octupole deformation softness in atomic nuclei, Phys. Rev. C 108 (2023) 024303, https://doi.org/10.1103/PhysRevC.108.024303.

[18] P.A. Butler, Octupole collectivity in nuclei, J. Phys. G: Nucl. Part. Phys. 43 (2016) 073002-26, https://doi.org/10.1088/0954-3899/43/7/073002.

[19] K.I. Arita, Semiclassical origin of nuclear ground-state octupole deformations, Phys. Rev. C 108 (2023) 044311-13, https://doi.org/10.1103/PhysRevC.108.044311.

[20] M. Dahlinger, E. Kankeleit, D. Habs, D. Schwalm, B. Schwartz, R.S. Simon, J.D. Burrows, P.A. Butler, Alternating

parity bands and octupole effects in ^{221}Th and ^{223}Th, Nucl. Phys. A 484 (1988) 337–375, https://doi.org/10.1016/0375-9474(88)90076-0.
[21] S. Ćwiok, W. Nazarewicz, Reflection-asymmetric shapes in transitional odd- A Th isotopes, Phys. Lett. B 224 (1989) 5–10, https://doi.org/10.1016/0370-2693(89)91039-3.
[22] C.F. Liang, P. Paris, R.K. Sheline, D. Trubert, C. Le Naour, M. Vergnes, Octupole deformation in ^{226}Th, Phys. Rev. C 57 (1998) 1145–1150, https://doi.org/10.1103/PhysRevC.57.1145.
[23] B. Buck, A.C. Merchant, S.M. Perez, Octupole bands in even isotopes of Ra, Th, U and Pu, J. Phys.: Conf. Ser. 111 (2008) 012041-6, https://doi.org/10.1088/1742-6596/111/1/012041.
[24] K. Nomura, D. Vretenar, B.-N. Lu, Microscopic analysis of the octupole phase transition in Th isotopes, Phys. Rev. C 88 (2013) 021303-5, https://doi.org/10.1103/PhysRevC.88.021303.
[25] N. Al-Dahan, Descriptive study of the even-even actinide nuclei ^{230} – ^{234}Th isotopes using IBM-1 Chinese, Phys. C 41 (2017) 064105-10, https://doi.org/10.1088/1674-1137/41/6/064105.
[26] I.M. Ahmed, M.A. Al-Jubbori, H.H. Kassim, H.Y. Abdullah, F.I. Sharrad, Investigation of even– even 220–230Th isotopes within the IBM, IVBM and BM, Nucl. Phys. A 977 (2018) 34–48, https://doi.org/10.1016/j.nuclphysa.2018.05.010.
[27] V.N. Tarasov, V.I. Kuprikov, D.V. Tarasov, Calculating the octupole deformation of radium and thorium isotopes in a Hartree–Fock–Bogolyubov approximation with skryme forces, Bull. Russ. Acad. Sci. Phys. 86 (2022) 998–1004, https://doi.org/10.3103/S1062873822080226.
[28] R.R. Guzmán, L.M. Robledo, Microscopic description of quadrupole- hexadecapolar coupling in radium, thorium, uranium, and plutonium isotopes with the Gogny energy density functional, Phys. Rev. C 111 (2025) 24304–24314, https://doi.org/10.1103/PhysRevC.111.024304.
[29] A. Arima, F. Iachello, Interacting boson model of collective states I. The vibrational limit, Ann. Phys. 99 (1976) 253–317, https://doi.org/10.1016/0003-4916(76)90097-X.
[30] A. Arima, F. Iachello, Interacting boson model of collective nuclear states II. The rotational limit, Ann. Phys. 111 (1978) 201–238, https://doi.org/10.1016/0003-4916(78)90228-2.
[31] A. Arima, F. Iachello, Interacting boson model of collective nuclear states IV. The $O(6)$ limit, Ann. Phys. 123 (1979) 468–492, https://doi.org/10.1016/0003-4916(79)90347-6.
[32] F. Iachello, A. Arima, The Interacting Boson Model, Cambridge University Press, Cambridge. 1987, https://doi.org/10.1017/CBO9780511895517.
[33] R.F. Casten, D.D. Warner, The interacting boson approximation, Rev. Mod. Phys. 60 (1988) 389–469, https://doi.org/10.1103/RevModPhys.60.389.
[34] A.F. Barfield, P. Von Brentano, A. Dewald, K.O. Zell, N.V. Zamfir, D. Bucurescu, M. Ivascu, O. Scholten, Evidence for the two-body nature of the E1 transition operator in the sdf-interacting boson model, Z. Phys. A Atomic Nuclei 332 (1989) 29–32, https://doi.org/10.1007/BF01292577.
[35] Y.X. Liu, H.Z. Sun, E. Zhao, Dynamical symmetries of the spdf interacting boson model, J. Phys. G: Nucl. Phys. 20 (1994) 407–424, https://doi.org/10.1088/0954-3899/20/3/003.
[36] N.V. Zamfir, D. Kusnezov, Octupole correlations in the transitional actinides and the spdf interacting boson model, Phys. Rev. C 63 (2001) 054306-9, https://doi.org/10.1103/PhysRevC.63.054306.
[37] N.V. Zamfi, D. Kusnezov, Octupole correlations in U and Pu nuclei, Phys. Rev. C 67 (2003) 014305-8, https://doi.org/10.1103/PhysRevC.67.014305.
[38] K. Nomura, D. Vretenar, T. Niksic, B.N. Lu, Microscopic description of octupole shape-phase transitions in light actinide and rare-earth nuclei, Phys. Rev. C 89 (2014) 024312-16, https://doi.org/10.1103/PhysRevC.89.024312.
[39] H.N. Qasim, F.H. Al-Khudair, Nuclear shape phase transition in even-even $^{158-168}$Hf isotopes, Nucl. Phys. A 1002 (2020) 121962-17, https://doi.org/10.1016/j.nuclphysa.2020.121962.
[40] K. Heyde, P. Van Isacker, M. Waroquier, J. Moreau, Triaxial shapes in the interacting boson model, Phys. Rev. C 29 (1984) 1420–1427, https://doi.org/10.1103/PhysRevC.29.1420.
[41] F.S. Radhi, A.A. Mohammed-Ali, A.H. Al-Musawi, Broken SU(3) Description of energy levels and decay properties in Gadolinium isotopes (A=156-160), Karbala International Journal of Modern Science 10 (2024) 485–496, https://doi.org/10.33640/2405-609X.3372.
[42] ENSDF, Nuclear data sheet. http://www.nndc.bnl.gov/ensdf, 2025.
[43] M.A. Al-Jubbori, H.H. Kassim, A.A. Abd-Aljbar, H. Y Abdullah, I. Hossain, I.M. Ahmed, F.I. Sharrad, Nuclear structure of the even–even rare-earth Er–Os nuclei for N=102, Indian J. Phys. 94 (2020) 379–390, https://doi.org/10.1007/s12648-019-01461-3.
[44] J. Stachel, P. Van Isacker, K. Heyde, Interpretation of the $A \approx 100$ transitional region in the framework of the interacting boson mode, Phys. Rev. C 25 (1982) 650–657, https://doi.org/10.1103/PhysRevC.25.650.
[45] K. Heyde, J.L. Wood, Shape coexistence in atomic nuclei, Rev. Mod. Phys. 83 (2011) 1467–1521, https://doi.org/10.1103/RevModPhys.83.1467.
[46] J.N. Ginocchio, M.W. Kirson, Relationship between the Bohrcollective Hamiltonian and the interacting boson model, Phys. Rev. Lett. 44 (1980) 1744–1747, https://doi.org/10.1103/PhysRevLett.44.1744.